Building Tomorrow's Society

Bâtir la Société de Demain

Fredericton, Canada

June 13 – June 16, 2018/ *Juin 13 – Juin 16, 2018*

STRENGTH AND DEFORMATION OF WELL-CONFINED GFRP-REINFORCED SHEAR WALLS

Hassanein, Ahmed[1], Nayera, Mohamed[2], Farghaly, Ahmed[3] and Benmokrane, Brahim[4,5]

[1] Doctoral student, Department of Civil Engineering, University of Sherbrooke, Sherbrooke, Quebec, Canada

[2] Former post-doctoral fellow, Department of Civil Engineering, University of Sherbrooke, Canada, Lecturer, Department of Civil Engineering, Assiut University, Egypt

[3] Research Associate, Department of Civil Engineering, University of Sherbrooke, Canada

[4] Professor, Department of Civil Engineering, University of Sherbrooke, Sherbrooke, Quebec, Canada

[5] Brahim.Benmokrane@usherbrooke.ca

Abstract: Well-detailed reinforced concrete shear walls are the most common lateral force-resisting system in reinforced concrete construction. The expected deformability and high lateral stiffness make them effective especially in high seismic regions. Recent studies have shown an acceptable level of strength and deformability of shear walls reinforced solely with glass fiber-reinforced-polymer (GFRP) bars. GFRP bars have emerged to be one of the most promising construction materials for reinforcing of different structural elements. Considering the aspects that still needed to fully understand this new seismic resistance system, the primary objective of the current study is to enhance the deformation capacity of the shear walls reinforced with GFRP bars. Three full-scale shear-wall specimens reinforced with GFRP bars were built and loaded to failure under cyclic lateral loads and constant axial load. The main objective of this study is to investigate the effect of the confinement configuration on the seismic behavior of the tested walls. The experimental results of the tested walls have showed an enhancement in the drift ratio and ultimate strength with the increase confinement level. In addition, the deformability factor (*J*) was assessed based on the experimental results.

1 INTRODUCTION

As a new application for glass fiber-reinforced-polymer (GFRP) reinforcement, full-scale shear walls reinforced with GFRP bars under cyclic loading were recently tested as a primary lateral-resisting system typically used for parking garages. The results show that the GFRP reinforced-concrete (RC) walls exhibited appropriate cyclic performance and possessed good deformation capacity in comparison to the steel-RC shear walls (Mohamed et al. 2014). Mohamed et al. (2014) carried out an experimental investigation of the applicability of reinforcing shear walls with GFRP bars in which the main parameters were steel versus GFRP reinforcing and different aspect ratios for GFRP-reinforced walls. The test matrix involved testing of four full-scale shear walls; one reinforced with steel bars and three with GFRP. Boundary-element reinforcement and diagonal bars were provided to eliminate sliding shear and ensure flexural domination. The test results showed that all of the tested walls achieved their predicted ultimate strength through flexural response, as evidenced by the typical amount of horizontal cracking. The observed failure mode was concrete crushing at one end associated with buckling of longitudinal bars for the steel-reinforced shear

wall and fracture of the longitudinal bars for the GFRP-reinforced shear walls. The observed cyclic response of the GFRP-reinforced walls showed insignificant strength degradation and reasonable stability of the wall stiffness. They achieved a higher drift ratio of 3.1% as compared to the steel wall's 2.6%. Due to the elastic behavior of the GFRP bars, the GFRP-reinforced shear walls achieved a lower level of deformability than the steel-reinforced wall (Mohamed et al. 2015).

In order to enhance the deformability behavior of the GFRP-reinforced shear walls, series of three full-scale shear walls were constructed with different confinement configurations at the boundary zone aiming to develop higher concrete strains at ultimate load and delaying the elastic–plastic transition point leading to the possibility to enhance the deformability performance of such walls.

2 EXPERIMENTAL PROGRAM

Three full-scale GFRP-reinforced concrete shear walls were tested under reversed quasi-static cyclic loading. Each specimen was tested under the combined action of constant axial load (15% of the axial wall capacity) and increasing reversed lateral load reversals. The methodology used for designing the test specimens is described. Material properties, cross-section and reinforcement details, the test setup, the predicted capacities were presented and discussed in detail in the following section.

2.1 Details of Test Specimens

The wall portion consisted of two boundary elements and two layers of vertical and horizontal web reinforcement. The spacing at the boundary element was selected such that adequate confinement to the concrete core would be provided and to delay longitudinal reinforcement buckling. Figure 1 shows the reinforcement details of the shear-wall specimens. The tested specimens had a dimension of 200 mm thickness, 1500 mm length, and 3500 mm height resulting in mid-rise shear walls. The wall base was 700 mm thick, 1200 mm width, and 2700 mm length. The three fabricated and tested GFRP-reinforced shear walls are denoted as; GX, GDC1, GDC2, where "G" stands for GFRP and "DC" stands for double confined boundary elements.

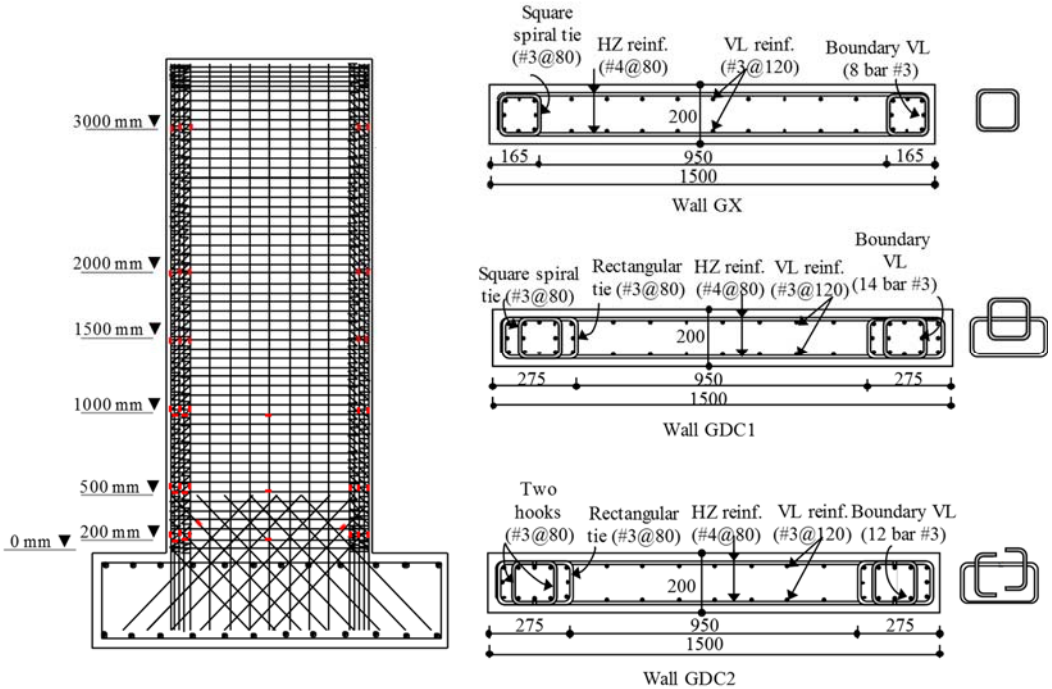

Figure 1: Concrete dimensions and reinforcement details

The specimens represent a model of a single shear wall complying with the special seismic requirements specified in CSA A23.3 (2014) and ACI 318 (2014) for the seismic-force resisting systems (SFRSs), as a case for new unexamined SFRS. The minimum thickness and reinforcement details were according to CSA S806 (2012) and ACI 440.1R (2006). The boundary element of specimen GDC1 had a square GFRP spiral embedded in the center of the rectangular spiral reducing the ties spacing to 40 mm. While, the boundary element of specimen GDC2 had two ties in the center of the rectangular spiral. Table 1 presents the dimensions and reinforcement ratios for all specimens.

Table 1 – Details of test specimens

Wall	f'_c MPa	l_b mm	l_{web} mm	ρ_b %	ρ_{web} %	ρ_h %	ρ_v %	V_f kN	V_r kN	V_r / V_f
GX	26.1	165	1170	1.73	0.55	1.58	4.0	469	671	1.43
GDC1	28.9	275	950	1.81	0.53	1.58	5.8	652	868	1.33
GDC2	24.3	275	950	1.56	0.53	1.58	5.0	571	754	1.32

f'_c = specified compressive strength, l_b = boundary length, l_{web} = web length, ρ_b = boundary long. Ratio, ρ_{web} = web long. Ratio, ρ_h = horizontal reinforcement ratio, ρ_v = boundary volumetric ratio

The predicted flexural strength (V_f) for the investigated walls was calculated based on plane-sectional analysis. The analysis was based on strain compatibility, internal force equilibrium, and the controlling mode of failure. The calculation was carried out considering the unconfined and confined concrete section. Sufficient shear reinforcement was provided to resist the shear force associated with the development of the probable moment resistance of the tested walls. The factored shear strength (V_r) was calculated as the sum of the shear resistance provided by the concrete and shear reinforcement according to CSA S806 (CAN/CSA 2012) equations (Clauses 8.4.4.5 to 8.4.4.11). The specimens were designed such that the ratio between theoretical flexural strength (V_f) and the theoretical shear strength (V_r) is more than 1.3 as presented in Table 1.

2.2 Materials

Sand-coated GFRP bars, spirals, and ties were used to reinforce the shear-wall specimens (Figure 2). The horizontal reinforcement comprised of #4 (12.7 mm diameter) GFRP bars spaced at 80 mm. The vertical reinforcement comprised of #3 (9.5 mm diameter) GFRP bars spaced at 120 mm. The boundaries were confined with different configuration for each specimen with GFRP #3 continuous spirals spaced at 80 mm, which is approximately the maximum spacing permitted in CSA S806 (2012).

Figure 2: GFRP reinforcement

The wall base was heavily reinforced with 25M Grade 60 deformed steel bars to avoid any base deformations intervening with the wall behavior. Table 2 lists the material properties of the reinforcing bars. The tensile properties of the longitudinal GFRP bars were determined according to ASTM D7205 (ASTM 2011). The wall portion was cast using normal-weight concrete with a target compressive strength of 30 MPa, the base was cast with higher concrete strength of 50 MPa. Table 1 gives the actual concrete

compressive strength based on the average values from the test performed on at least five 100 × 200 mm cylinders for each wall on one day before testing of the shear-wall specimen.

Table 2 – Mechanical properties of reinforcement

Bar	d_b	A	E_f	f_{fu}	ε_f
Straight bars					
GFRP #3	9.5	71.3	62.5	1346	2.30
GFRP #4	12.7	126.7	61.3	1303	2.35
Bent bars					
GFRP #3	Straight portion		52	962	1.85
	Bent portion		--	500	--

d_b: bar diameter (mm), A: area (mm^2), E_f: Modulus of elasticity (GPa), f_{fu}: Tensile strength (MPa), ε_f: Tensile strain (%)

2.3 Test Setup and Procedure

A series of linear variable differential transducers (LVDTs) and strain gauges were used to measure critical response quantities. That notwithstanding, only the instruments used in this study is shown (Figure 3). Lateral displacement was measured at the top of the wall height; two LVDTs were used to measure horizontal sliding between the wall and base as well as between the base and the rigid floor. An automatic data-acquisition system monitored by a computer was used to record the LVDT and load-cell readings. During loading, crack propagation was marked and recorded.

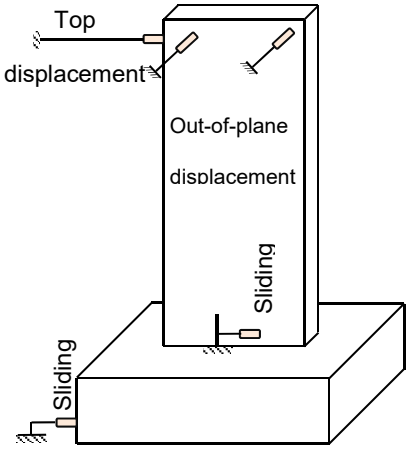

Figure 3: LVDTs configuration

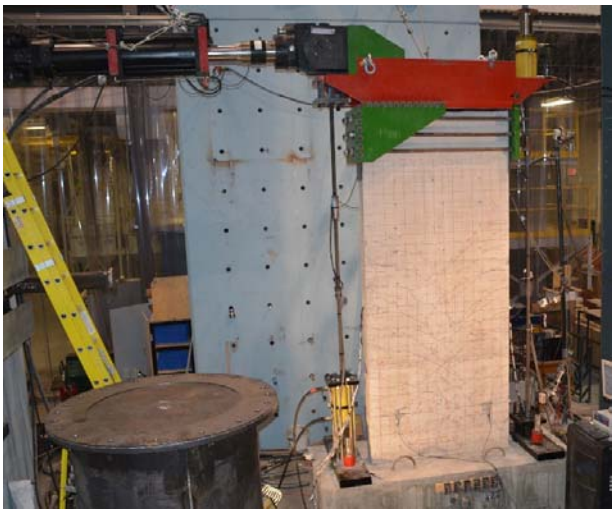

Figure 4: Test setup

Figure 4 shows the test setup. The wall specimens were tested in an upright position. A specially fabricated steel load-transfer assembly was used to transfer both axial and lateral loads to the wall specimen. An axial load of approximately $0.15 b_w l_w f_c'$ was applied at the top of the wall by two hydraulic jacks mounted to the load-transfer assembly. The SEAOC (2009) stated that the maximum allowable axial load stress for seismic resisting systems shall not exceed 15% of the permissible axial stress. This axial load limit assures sufficient ductility or lateral stability when the wall hinges at the base. The axial stress was maintained constant throughout the duration of each test. Cyclic lateral displacements were applied to the walls with a 1000 kN MTS actuator mounted horizontally to a reaction wall. Out-of-plane bracing was provided to prevent out-of-plane displacement, simultaneously providing no resistance to in-plane displacement. As the loading history was not a test variable, a typical procedure of applying quasi-static reversed cyclic loading was adopted for all test specimens (Figure 5). The walls were cycled twice at each displacement level with increments of 2 mm up to 10 mm, followed by increments of 5 mm up to 50 mm, and then increments of 10 mm to failure. Hinged connections at the tips of both the horizontal actuator and vertical hydraulic jacks prevented any substantial restraint of rotation of the top of the wall, thus ensuring cantilever behavior.

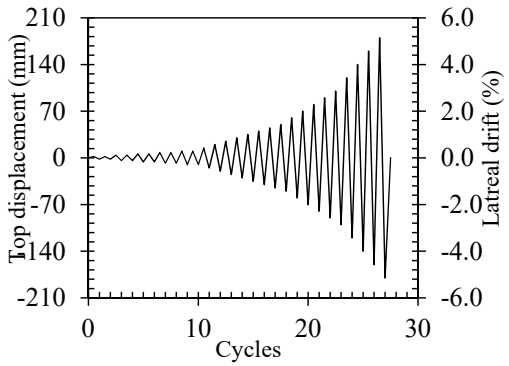

Figure 5: Loading History

3 EXPERIMENTAL RESULTS

Overall, the three walls achieved their flexural strength with no sign of strength decay up to failure. The first horizontal crack appeared at the lower part of the wall at approximately 0.22% drift when the lateral load reached (V_{cr}) as presented at table 3. It can also be noted that the three walls had initial stiffness nearly similar until initial crack formation when a reduction of stiffness was clearly observed at two different levels

for each wall. In the following cycles, several new horizontal cracks appeared above the first crack and developed upward the wall height. Flexural cracks extended to about two thirds of the height of the wall (2/3 l_w). These cracks developed into inclined flexural-shear cracks. The cracking pattern at the end of the test is shown in Figure 6. The inclination of the shear cracks was quite higher in the top part than that of the cracks at the bottom part. Vertical splitting cracks (shown in Figure 7a) typically appeared at the boundaries when the concrete compression strain ranged between 0.003 to 0.0035 (corresponding to drift ranged between 0.7 and 0.8%) at a lateral strength levels denoted as V_{split} in table 3. With cycling to a higher displacement level, the pieces of concrete between the intersecting cracks gradually fall and spalling of concrete cover occurred at both sides of boundary elements (Figure 7b) at a lateral load level of $V_{spalling}$ in Table 3. The measured lateral displacements indicated that the specimens were able to sustain a drift ratio of at least 3.2% without strength degradation. As expected, the walls with higher confinement ratios achieved at least 30% more drift and sustained at least 25% more lateral strength due to the confinement efficiency in increasing the ultimate concrete compressive strain in the boundary elements zone.

Table 3 – Experimental results

Wall	V_{cr}	V_{split}	$V_{spalling}$	V_u	ε_{cu}	δ_u
GX	176	318	385	475	0.013	3.23
GDC1	187	344	436	693	0.016	4.46
GDC2	161	309	422	594	0.015	4.19

V_{cr}: load corresponding to first crack (kN), V_{split}: load corresponding to concrete cover splitting (kN), $V_{spalling}$: load corresponding to concrete cover spalling (kN), V_u: experimental ultimate load (kN), ε_{cu}: concrete compression strain at failure, δ_u: drift values corresponding to ultimate load calculated as the lateral displacement to wall height.

The observed failure mechanism for the tested walls was similar despite the difference in confinement configuration with the following sequence: (i) rupture of the spiral in the compressed boundary element leading to a slight degradation in the axial and lateral strengths (Figure 7c), (ii) lateral displacement continued to increase with almost constant lateral load, (iii) vertical bar fracture was recorded associated with rupture of another spiral and concrete crashing of the boundary-element core reveling the domination of the flexure mode of failure.

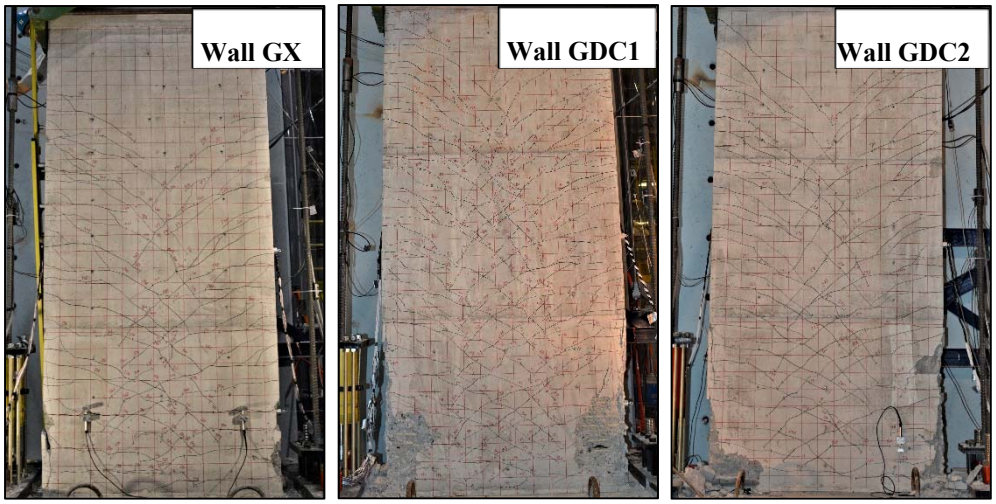

Figure 6: Crack patterns

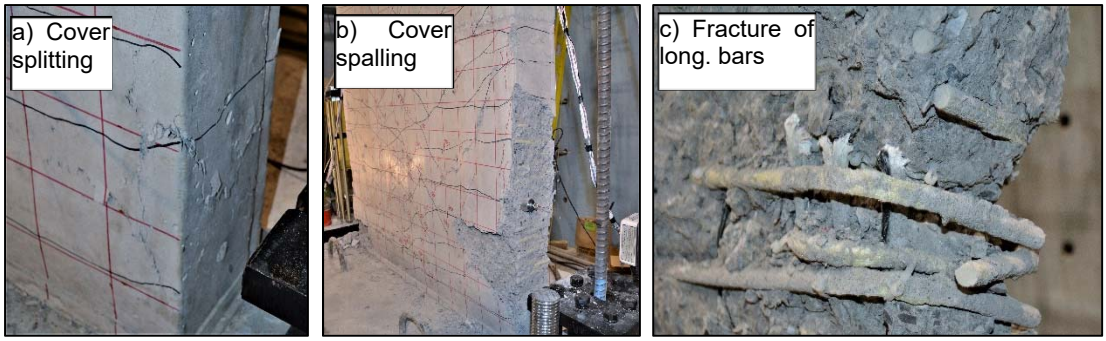

Figure 7: Failure progression at the boundary element

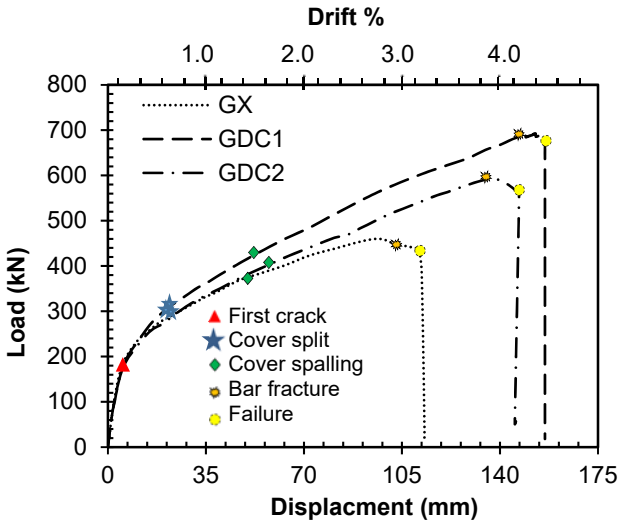

Figure 8: Half-cycle envelope curves

Figure 8 shows the envelop curves of the hysteretic response, and due to the symmetric response in both load directions, only the half cycles of the load-displacement curves is presented. It can be observed that the first crack initiated at the same level of displacement, also the cover splitting and spalling were observed at a similar displacement level for the three tested walls. When the walls reached its ultimate capacity, the fracture of the longitudinal bar in the extreme compression side caused a strength decay. Moreover, it can be observed that the strength decay followed by an increase in the displacement until failure. The level of strength achieved was 475, 693, and 594 kN for the walls GX, GDC1 and GDC2, respectively.

The calculated flexural capacities given in Table 1 are in good agreement with the experimentally recorded ultimate strength (Table 3) demonstrating the applicability in using the plan-sectional analysis to predict the flexural capacity of GFRP-reinforced concrete walls.

4 DEFORMATION CAPACITY

Ductility is the measure of the wall ability to deform beyond yielding of the flexural reinforcement. However, the FRP bars are elastic material in nature and they do not exhibit yielding. Therefore, the new term “deformability” was proposed by Jaeger et al. (1995) to have the ability to assess the deformation level of the FRP-reinforced shear walls based on deformability and strength considerations instead of ductility. Since concrete members reinforced with FRP bars are highly deformable, structures should be designed based on a curvature factor. The curvature factor is the ratio of curvature at the ultimate state to the curvature at a concrete strain of 0.001 (Jaeger et al. 1995). Moreover, the strength factor is also considered

which is defined as the ratio of ultimate moment to moment at a concrete strain of 0.001 (Jaeger et al. 1995). To take these two factors into account, Jaeger et al. (1995) defined an overall deformability factor (*J*) calculated as the product of the curvature factor and strength factor expressed as follows:

$$[1]\ J = \frac{M_u}{M_c}\frac{\phi_u}{\phi_c}$$

where *M* and *Φ* are moment and curvature at service or ultimate load, denoted by the subscripts *c* or *u*, respectively. The Canadian Highway Bridge Design Code includes an overall performance factor for FRP-RC beams and slabs (CSA S6-06) that combines the strength and deformability given by Eq. 1 with the service condition taken as the point at which the maximum concrete compressive strain reaches 0.001. Therefore, the concrete compression-strain limit of 0.001 was chosen to represent linear stress–strain behavior in compression and to define the serviceability limit state.

However, In the current tested GFRP-reinforced shear walls, the concrete compression strain reached more than 0.013 at ultimate for wall GX and more than 0.015 for walls GDC1 and GDC2. Similar results were reported in Mohamed et al. (2014). Therefore, the concrete compression-strain limit of 0.001 is very conservative and produces relatively high values of $J_{0.001}$ as shown in Table 4. The deformability factor (*J*) was recalculated based on the moment and the curvature corresponding to the concrete compressive strain equal to 0.003, which reflect the initiation of the inelastic deformations in the tested walls based on the definition of CSA S6-06. Table 4 provides the calculated values of the deformability factor (*J*) for the tested walls. Due to the difference in the values of the moments and the curvatures corresponding to concrete compressive strains of 0.001 and 0.003, a clear difference between the two procedures resulted in unreliably high values for the deformability factor ($J_{0.001}$) compared to the ($J_{0.003}$). The calculated deformability factor ($J_{0.003}$) show the enhancement in deformability capacity due the higher level of confinement in the boundary element zone.

Table 4 – Deformability factor

Wall	$\Phi_{0.001}$	$M_{0.001}$	$\Phi_{0.003}$	$M_{0.003}$	Φ_u	M_u	$J_{0.001}$	$J_{0.003}$
	Rad/m	*kN.m*	*Rad/m*	*kN.m*	*Rad/m*	*kN.m*		
GX	0.0022	853	0.0069	1212	0.0256	1896	25.9	5.8
GDC1	0.0026	832	0.0079	1422	0.0340	2805	41.1	8.5
GDC2	0.0023	799	0.0071	1256	0.0317	2285	42.3	8.1

5 CONCLUSIONS

The main aspects that were investigated by means of these tests concern the effects of the reinforcement content and configuration in the boundary element on the deformation behavior of the GFRP-reinforced shear walls. Based on the experimental results, the following conclusions can be addressed;

1. Increasing the level of confinement in the boundary element zone of GFRP-reinforced shear walls has significantly enhanced the strength and deformation capacities under reversed cyclic loading.

2. The shear wall reinforced with GFRP bars can achieve a drift ratio up to 4.4 %, which is beyond the required drift limits in most seismic design codes (NBCC 2010).

3. The deformability factor (*J*) is recommended to be calculated based on the moment and curvature corresponding to the ultimate state and the to the concrete compressive strain of 0.003.

4. More experimental and analytical studies are needed to further validate the present findings and to study the effect of different reinforcement ratios on the performance of shear walls reinforced with FRP bars.

Acknowledgements

The authors wish to acknowledge the financial support of the Natural Sciences and Engineering Research Council of Canada (NSERC), the Canada Research Chair in Advanced Composite Materials for Civil Engineering, and the Fonds québécois de la recherche – Nature et Technologies - (FQRNT) of Quebec.

References

ACI Committee 318. Building Code Requirements for Structural Concrete and Commentary (ACI 318-14). American Concrete Institute, Farmington Hills, MI, 2014, 473 pp.

ACI Committee 440. Guide for the Design and Construction of Concrete Reinforced with FRP Bars (ACI 440.1R-06). American Concrete Institute, Farmington Hills, MI, 2006, 44 pp

ASTM D7205 / D7205M – 06. 2011. Standard Test Method for Tensile Properties of Fiber Reinforced Polymer Matrix Composite Bars, 13 pp.

CSA A23.3. Design of Concrete Structures Standard. Canadian Standards Association, Mississauga, ON, Canada, 2014, 240 pp.

CSA S806. Design and Construction of Building Components with Fiber-Reinforced Polymers. Canadian Standards Association, Mississauga, ON, Canada, 2012, 208 pp.

CSA-S6-06. Supplement #1 to Canadian Highway Bridge Design Code (CAN/CSA S6S1-10), Canadian Standards Association, Mississauga, ON, Canada, 2006, 1078 pp.

Jaeger L.G., Tadros G. and Mufti A.A. 1995. Balanced Section, Ductility and Deformability in Concrete with FRP Reinforcement. Technical Report No.2-1995, CAD/CAM Centre. Technical University of NS, Halifax.

Mohamed, N., Farghaly, A. S., Benmokrane, B. and Neale, K. W. 2014. Experimental Investigation of Concrete Shear Walls Reinforced with Glass-Fiber-Reinforced Bars under Lateral Cyclic Loading. ASCE Journal of Composites for Constructions, 18 (3): A4014001.

Mohamed, N., Farghaly, A. S. and Benmokrane, B. 2015. Aspects of Deformability of Shear Walls Reinforced with GFRP bars. ASCE Journal of Composites for Constructions, 19 (5): 06014001.

National Building Code of Canada. Canadian Commission on Building and Fire Codes (NBCC). National Research Council of Canada, Canada, 2010.

SEAOC, 2009, SEAOC Blue Book: Seismic Design Recommendations, Structural Engineers Association of California, Sacramento, California.